NeuroImage: Clinical 29 (2021) 102571

Contents lists available at ScienceDirect

NeuroImage: Clinical

journal homepage: www.elsevier.com/locate/ynicl

Homotopic redistribution of functional connectivity in insula-centered diffuse low-grade glioma

Fabien Almairac [a,b], Jeremy Deverdun [c,d], Jérôme Cochereau [e,f,g], Arthur Coget [c,d], Anne-Laure Lemaitre [h], Sylvie Moritz-Gasser [f,g,h], Hugues Duffau [f,g,h], Guillaume Herbet [f,g,h,*]

[a] Department of Neurosurgery, Pasteur 2 Hospital, Nice University Medical Center, Nice, France
[b] Université Côte d'Azur, Nice, France
[c] I2FH, Institut d'Imagerie Fonctionnelle Humaine, Gui de Chauliac Hospital, Montpellier University Medical Center, Montpellier, France
[d] Department of Neuroradiology, Gui de Chauliac Hospital, Montpellier University Medical Center, Montpellier, France
[e] Department of Neurosurgery, La Miletrie Hospital, Poitiers University Medical Center, Poitiers, France
[f] Institute of Functional Genomics, INSERM 1191, University of Montpellier, France
[g] University of Montpellier, Montpellier, France
[h] Department of Neurosurgery, Gui de Chauliac Hospital, Montpellier University Medical Center, Montpellier, France

ARTICLE INFO

Keywords:
Insula
Plasticity
Glioma
Homotopic
Functional MRI
Functional connectivity

ABSTRACT

Objective: In the event of neural injury, the homologous contralateral brain areas may play a compensatory role to avoid or limit the functional loss. However, this dynamic strategy of functional redistribution is not clearly established, especially in the pathophysiological context of diffuse low-grade glioma. Our aim here was to assess the extent to which unilateral tumor infiltration of the insula dynamically modulates the functional connectivity of the contralesional one.

Methods: Using resting-state functional connectivity MRI, a seed-to-ROI approach was employed in 52 insula-centered glioma patients (n = 30 left and 22 right) compared with 19 age-matched healthy controls.

Results: Unsurprisingly, a significant decrease of the inter-insular connectivity was observed in both patient groups. More importantly, the analyses revealed a significant increase of the contralesional insular connectivity towards both cerebral hemispheres, especially in cortical areas forming the visual and the sensorimotor networks. This functional redistribution was not identified when the analyses were performed on three control regions for which the homologous area was not impaired by the tumor. This overall pattern of results indicates that massive infiltration of the insular cortex causes a significant redeployment of the contralesional functional connectivity.

Conclusion: This general finding suggests that the undamaged insula plays a role in the functional compensation usually observed in this patient population, and thus provides compelling support for the concept of homotopic functional plasticity in brain-damaged patients.

1. Introduction

The human insula is a cortical structure known to be involved in a vast number of homeostatic, cognitive and affective processes. It may act as a multisensory interfacing center, since it receives all kinds of sensory, motor and visceral inputs (Nieuwenhuys, 2012). Furthermore, insular structures are strongly engaged in a wide panel of cognitive processes including body awareness, self-recognition, interoception, emotional awareness, and salience ((Bud) Craig, 2009; Uddin, 2015). Such a pivotal role in functional organization is unsurprisingly supported by a complex connective architecture, as observed *in vivo* with the use of diffusion tractography, functional MRI (fMRI) and cortico-cortical evoked potentials (CCEPs) (Cauda et al., 2011; Cerliani et al., 2012; Dionisio et al., 2019).

Despite the highly integrative feature of the insular cortex, its injury does not necessarily result in the range of neuropsychological or neurological impairments one would expect, especially in the event of graded damage as in diffuse low-grade glioma (DLGG) (Duffau, 2005;

* Corresponding author at: Department of Neurosurgery, Hôpital Gui de Chauliac, Institute of Functional Genomics, INSERM 1191, University of Montpellier, 80 avenue Augustin Fliche, 34295 Montpellier, France.
E-mail address: guillaume.herbet@gmail.com (G. Herbet).

https://doi.org/10.1016/j.nicl.2021.102571
Received 12 July 2020; Received in revised form 12 January 2021; Accepted 13 January 2021
Available online 19 January 2021
2213-1582/© 2021 The Author(s). Published by Elsevier Inc. This is an open access article under the CC BY-NC-ND license (http://creativecommons.org/licenses/by-nc-nd/4.0/).

Duffau et al., 2006; Herbet et al., 2016). Different neuroplasticity strategies may account for such an efficient functional compensation, including loco-regional, intra-hemispheric and inter-hemispheric functional redistributions (Coget et al., 2018; Desmurget et al., 2007). Furthermore, recent studies indicate that the contralesional, homotopic structures may play a strategic role (Gauthier et al., 2008; Voytek et al., 2010), especially in the context of bi-lateralized networks (Rice et al., 2018). The evidence remains, however, preliminary. In that respect, a recent morphometry study performed by our research group demonstrated an increase of gray matter density in the contralesional insula in response to the tumor infiltration of the ipsilesional one (Almairac et al., 2018). We hypothesized that macrostructural changes of the homotopic insula may support the efficient functional compensation generally observed in these patients - these changes being probably paralleled by a redistribution of functional connectivity. However, to date, this lesion-induced 'homotopic' redistribution of functional connectivity has not been investigated.

In this study, we aimed to assess the extent to which widespread unilateral tumor infiltration of the insula dynamically modulates the functional connectivity of the contralesional one, capitalizing on a large and strictly selected sample of insula-centered DLGG patients.

2. Materials and methods

2.1. Participants

We retrospectively included 52 patients (mean age 41.1 ± 10.2 years [range: 21–63]; 25 women) with a DLGG centered on the left ($n = 30$, "insL" group) or right ($n = 22$, "insR" group) insula, over a period of five years (2012–2017) at the Montpellier University Hospital (Table 1). In order to select a homogenous sample of patients with a slow-growing, low-grade glioma, allowing time for functional reorganization to occur, we only included unifocal grade II IDH-mutated gliomas (astrocytoma and oligodendroglioma) according to the WHO 2016 classification (Louis et al., 2016). To prevent any epileptic seizure in the perioperative period, all the patients were treated with levetiracetam, and therefore has the fMRI measurements under treatment. This antiepileptic drug may affect the intra-network connectivity (Pang et al., 2020). Patients with a high-grade glioma (grade > II) and/or IDH wild-type, previous treatment for their brain tumor (brain surgery, chemotherapy or radiotherapy), a multifocal glioma or bilateral extension of the glioma, other intracranial abnormalities, brain midline shift due to tumor volume, MRI acquisition or preprocessing issues were excluded at the outset. The healthy control group (hereafter, 'HCs') was composed of 19 age-related participants from a local database (Yordanova et al., 2019) (Table 1).

The 3 groups (insL, insR, HCs) were comparable in terms of age ($F_{2,68} = 0.17$, $p = 0.85$), sex ($\chi^2 = 0.99$, $p = 0.61$) and handedness ($\chi^2 = 4.78$, $p = 0.09$), but not for scanner type ($\chi^2 = 7.19$, $p = 0.028$) and tumor volume ($t_{48} = 2.03$, $p = 0.048$).

Table 1
Demographic data and further covariates.

Variable	Patients		HCs	*p* values
	InsL	InsR		
No.	30	22	19	NA
Age (mean ± SD), years	40.9 ± 8.5	41.6 ± 12.3	42.7 ± 11.7	0.845
Sex ratio, F/M	16/14	9/13	8/11	0.610
Handedness, R/L, n	26/4	17/5	19/0	0.092
Scanner type, 3 T/1.5 T, n	27/3	16/6	19/0	**0.028**
Tumor volume, cm^3	69.3 ± 34	51.1 ± 30.4	NA	**0.048**

Abbreviations: HC = healthy control; InsL = left insular glioma; insR = right insular glioma; L = left-handed; NA = not applicable; R = right-handed. The *p* values were determined by a one-way analysis of variance for age, a χ^2 test for sex ratio, handedness and scanner type, and a *t*-test for tumor volume.

2.2. Standard protocol approvals, registrations, and patient consents

This study was conducted in compliance with the ethics standards of our institution for a retrospective study. All patients gave their informed consent to the retrospective extraction of clinical and imaging data from their medical files. All healthy control participants provided written consents (IRB: 2010-AZ-1313–36).

2.3. Image acquisition

Structural and functional imaging sequences were acquired in the same Neuroimaging Department with a 1.5 T (Avanto) or a 3 T (Skyra) MRI Siemens scanner (Siemens, Erlangen, Germany), using a 32-channel head coil, as part of the patients' care protocol. For this study, we used (1) high-resolution 3DT1 as structural images for co-registration with functional images of the resting-state functional MRI (rsfMRI); (2) A rsfMRI session using T2*-weighted GE-EPI (gradient echo – echo-planar imaging) acquisition in which patients were asked to keep their eyes closed, to relax and to think to nothing in particular; (3) An axial FLAIR (fluid-attenuated inversion recovery) sequence to delineate the lesions as this sequence yields the best contrast between normal and infiltrated brain parenchyma. All control participants ($n = 19$) and the majority of the patients ($n = 43/52$, 27 insL, 16 insR) performed the MRI on the 3 T machine. The use of different scanners was not related to the purpose of the study but was due to the renewal of the previous scanner in our medical center. However, to account for its potential effects on resting-state functional connectivity, we included the between-scanner difference as a covariate in the analyses (Coget et al., 2018).

2.4. Imaging protocol

The specifications of the acquisition were as follows for: (1) 3DT1 images (1.5 T/3T parameters): repetition time (TR) 1880/1700 ms, echo time (TE) 3.4/2.5 ms, inversion time 1100/922 ms, field of view 256 × 256 mm, voxel size 1 × 1 × 1 mm^3, 176 axial slices, and flip angle 15°/9°; (2) RsfMRI session (1.5 T/3T parameters): TR 2320/2400 ms, TE 50/30 ms, voxel size 3 × 3 × 5.5/2.39 × 2.39 × 3 mm^3, 28/39 interleaved slices, 200 whole-brain volumes, flip angle 90°, and acquisition duration 8.07 min; (3) FLAIR images (1.5 T/3T parameters): TR 13200/800 ms, TE 109/108 ms, inversion time 2500/23700 ms, field of view 210 × 240/202 × 240 mm, voxel size 0.898 × 0.898 × 6 mm^3, slice thickness 5/3 mm, spacing 5.5/3.6 mm, and flip angle 150°.

2.5. RsfMRI pre-processing

The following preprocessing steps were achieved using the CONN Toolbox (functional connectivity toolbox, release 18.b) (Whitfield-Gabrieli and Nieto-Castanon, 2012) under MATLAB environment (release 2019a, The MathWorks, Inc., MA, USA). We performed the 'default preprocessing pipeline for volume-based analyses with direct normalization to MNI-space' preceded by the step 'functional removal of initial scans' in order to remove the first five volumes of the rsfMRI session for each participant; this allows to reach a steady state due to initial patients' movements. That pipeline performs a separate normalization (non-linear transformation to MNI space) of the structural and functional data. Note that, based on previous study of our group (Cochereau et al., 2016; Yordanova et al., 2019), the normalization process was performed without tumor masking, and that each normalized image was systematically and carefully checked to exclude inconsistent deformations. This approach was motivated by the fact that DLGG are, due to their invasive and slow growth pattern and in contrast to high-grade glioma and stroke, much less prone to mass effects. Briefly, from the corresponding structural and functional files, the preprocessing pipeline covered the following steps: removal of the first five volumes of the rsfMRI session, realignment and unwarp and phase correction, translation to functional and structural center (0,0,0) coordinates, slice-

timing correction, outlier detection, direct segmentation and normalization to a common stereotactic Montreal Neurological Institute (MNI) space, co-registration of the functional and structural normalized volumes, and functional volume smoothing using a 8-mm isotropic Gaussian filter. Then, the CONN's default denoising pipeline was performed on data in order to remove unwanted motion, physiological and other artefactual effects from the BOLD signal before computing connectivity measures. It consists on applying a linear regression of potential confounding effects in the BOLD signal which are estimated and removed separately for each voxel and for each subject, using Ordinary Least Squares (OLS) regression. The denoising process implements an anatomical component-based noise correction procedure (aCompCor), and includes noise components from cerebral white matter and cerebrospinal areas (Behzadi et al., 2007), estimates subject-motion parameters (12 potential noise components) (Friston et al., 1995), and a scrubbing of identified outlier scans (Power et al., 2014). Also, to minimize the influence of physiological, head-motion and other noise sources, a temporal band-pass filter (0.008 – 0.09 Hz) was applied. After regression, a discrete cosine transform windowing operation to minimize border effects was performed (Hallquist et al., 2013).

2.6. Seed-to-ROI and seed-to-network analyses

In the first-level analysis, a general linear model (GLM) was computed by the CONN Toolbox (for more details, please refer to https://web.conn-toolbox.org/fmri-methods/general-linear-model). Then, a ROI-to-ROI connectivity matrix was generated for each participant using the weighted GLM for weighted regression/correlation measures of the association between the seed/source BOLD timeseries and each target ROI BOLD timeseries. The ROI-to-ROI connectivity (RRC) matrix was created by the CONN Toolbox. Each element in the RRC matrix was defined as the Fisher-transformed bivariate correlation coefficient between a pair of ROI BOLD timeseries, as explained in more details here (https://web.conn-toolbox.org/fmri-methods/connectivity-measures/roi-to-roi). Bivariate correlation coefficients were converted to normalized z-scores using Fisher's transform to allow subsequent GLM analyses. Note that the ROI map of the CONN toolbox is extracted from the FSL Harvard-Oxford Atlas, covering 91 cortical and 15 subcortical structural areas (Desikan et al., 2006), and the 7 commonly used supratentorial functional networks defined from CONN's independent component analyses of Human Connectome Project dataset (497 subjects): Default Mode Network (4 ROIs), SensoriMotor (3 ROIs), Visual (4 ROIs), Salience / Cingulo-Opercular (7 ROIs), DorsalAttention (4 ROIs), FrontoParietal / Central Executive (4 ROIs), and Language (4 ROIs). Then, second-level analysis was conducted for both patient groups (insL and insR), and for HCs. The seed-ROIs were the right or left insula extracted from the FSL Harvard-Oxford Atlas in the CONN Toolbox interface. As we excluded patients with a midline shift due to tumor volume, no mass effect occurred in the contralesional hemisphere, allowing to position the insula seed-ROI confidently. In the second-level analysis, we used an ANCOVA covariate control model (between-subjects contrast), adding age and scanner-type as nuisance covariates ([1 −1 0 0]). ROIs functionally related to the "insular cortex" seed were identified with a two-sided threshold set at $p < 0.05$ applying a FDR correction (false discovery rate) (Glickman et al., 2014) to correct for multiple comparisons across all possible target ROIs. For the seed-to-ROI analysis, the dimension of the connectivity matrix was 106x106 (91 cortical and 15 subcortical structural areas). For the seed-to-network analysis, the dimension of the connectivity matrix was 32x32 (the two insular cortex areas, and the 30 ROIs belonging to the 7 functional networks).

2.7. Control ROIs

In order to assess the specificity of the results related to the insular cortex, we selected three control regions from the FSL Harvard-Oxford Atlas, using the same method as described above. This included the anterior inferior temporal gyrus (aITG), the posterior temporal fusiform cortex (pTFusC), and the middle frontal gyrus (MidFG). This selection was driven by the fact that the three regions were spared by tumor infiltration and poorly connected to the insula according to parcellation studies (Cauda et al., 2011). Consequently, we could hypothesize that they would be little or not at all affected by the insula-related functional redistribution. The results obtained with each control ROI was examined separately for both patient groups compared with HCs.

2.8. Lesion drawing

To define anatomically the lesion of each patient, we delineated the tumor on FLAIR images because it allows the best difference in contrast between the healthy and the lesioned tissue, as previously reported (see Supplementary Fig. 1) (Almairac et al., 2018, 2015, Herbet et al., 2016). More specifically, original FLAIR images were first normalized to the MNI space with SPM12 using a spatial resolution of $1 \times 1 \times 4$. Then, the tumors were traced manually by hands by the first author using MRIcron software (https://www.nitrc.org) (Rorden et al., 2007). The resulting maps were systematically checked by the senior author who has a solid background in neuroanatomy. Lesion overlap maps are displayed in Fig. 1A and B. Tumor volumes were automatically generated with MRIcron from the lesion drawing.

2.9. Data availability statement

Anonymized data will be shared by request from any qualified investigator.

3. Results

Analyses were performed in 52 insula-centered glioma patients ($n = 30$, insL; $n = 22$, insR) statistically contrasted with 19 age-matched healthy controls (Table 1). In both patient groups (insL and insR), the maximum lesion overlap occurred in the insula (Fig. 1A and B, respectively).

The group-level comparison of insL with HCs revealed an increase of resting-state functional connectivity (rsFC) between the right, contralesional insular cortex and four cortical areas belonging to both the left and right hemisphere, mainly including occipital and parietal regions, as well as a decreased rsFC with the lesional insular cortex (Fig. 2A, and Supplementary Table 1). The seed-to-network analysis identified an increase of the contralesional insular rsFC with 2 functional networks in insL patients compared with HCs, including the bilateral visual (lateral and medial) and the superior sensorimotor network (Fig. 2B, and Supplementary Table 2).

In the same group of patients, we found unsurprisingly a significant decrease of rsFC between the left, ipsilesional insular cortex and 12 central and anterior cortical areas distributed in both hemispheres as well as an increased rsFC with the left middle temporal gyrus (Fig. 2C, and Supplementary Table 3). The seed-to-network analysis identified a decrease of the ipsilesional insular rsFC with 3 functional networks in insL patients compared with HCs, mainly including the bilateral salience and the lateral sensorimotor networks (Fig. 2D, and Supplementary Table 4).

The comparison of insR with HCs revealed similar results; an increased insular rsFC of the left, contralesional insular cortex was mainly observed with posterior cortices (temporal, occipital, parietal), and sensorimotor regions in both cerebral hemispheres, as well as with the right frontal pole cortex ($n = 15$ ROIs). A decreased rsFC with the lesional insular cortex was also evidenced in this patient group (Fig. 3A, and Supplementary Table 5). In agreement with this, the seed-to-network analysis identified an increase of the contralesional insular rsFC with areas of 2 functional networks, including the visual and the superior sensorimotor networks in both cerebral hemispheres (Fig. 3B,

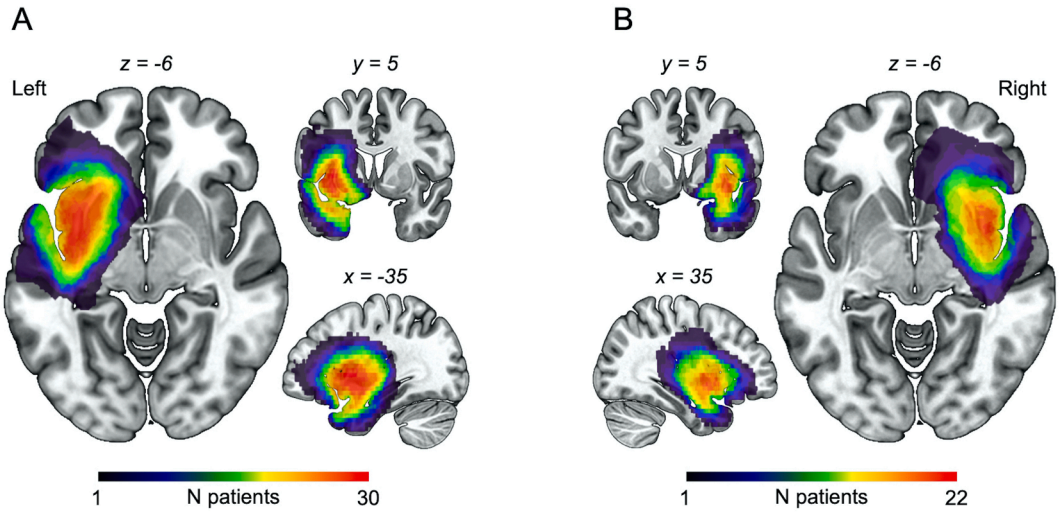


Fig. 1. Lesion overlap map for (A) left insular glioma and (B) right insular glioma patients. As expected, the maximum overlap occurred in the insula.

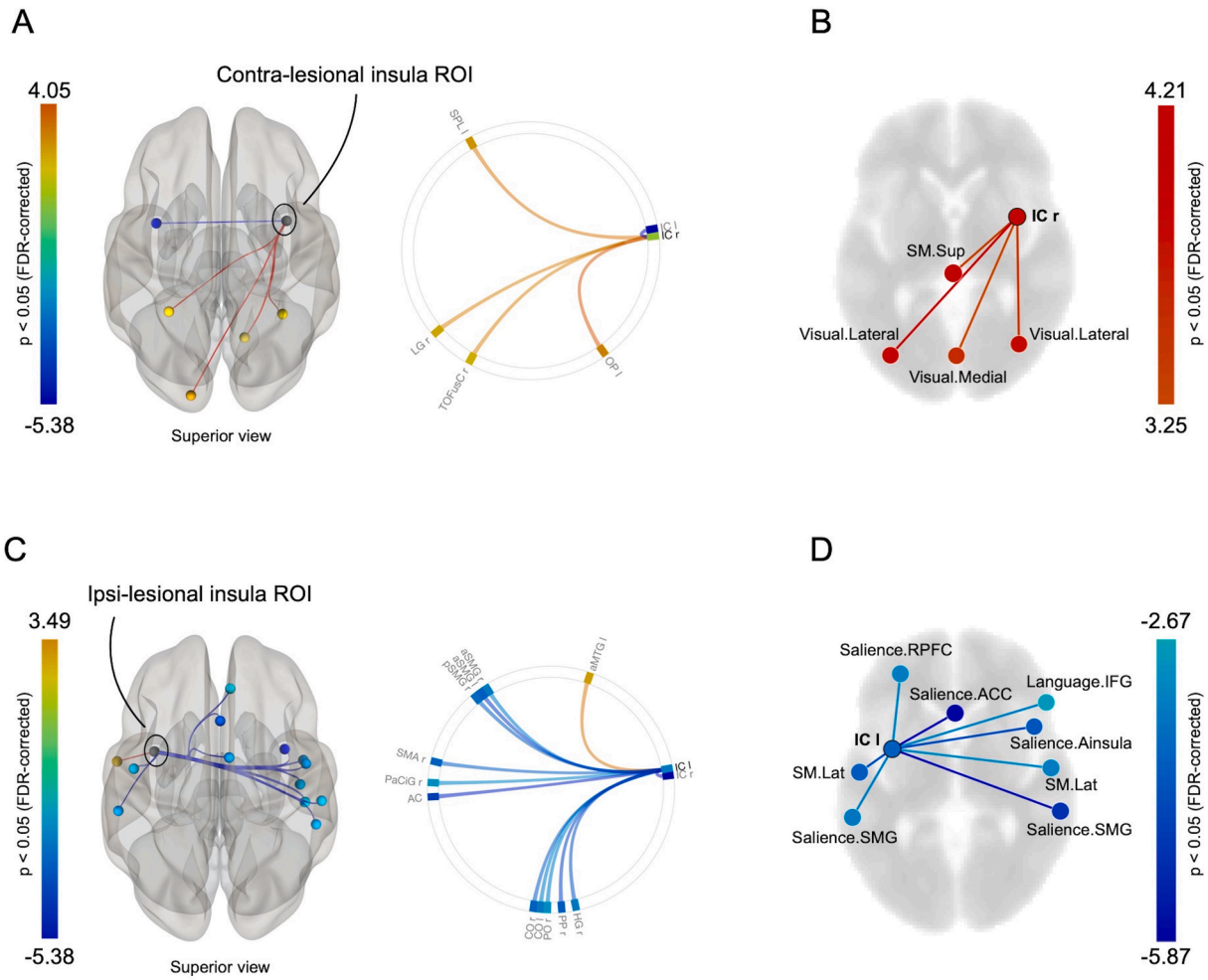


Fig. 2. Tumor-related modulation of insular connectivity in left insular glioma patients versus healthy controls. (A) Contralesional insula seed-to-ROI map and connectome ring. (B) Contralesional seed-to-network map displayed on an axial slide. (C) Ipsilesional insula seed-to-ROI map and connectome ring. (D) Ipsilesional insula seed-to-network map displayed on an axial slide. Only significant T-values ($p < 0.05$ FDR-corrected) are displayed. ACC = anterior cingulate cortex; IC = insular cortex; IFG = inferior frontal gyrus; FDR = false discovery rate; RPFC = rostral prefrontal cortex; SM.Lat = lateral sensorimotor; SM.Sup = superior sensorimotor; SMG = supramarginal gyrus.

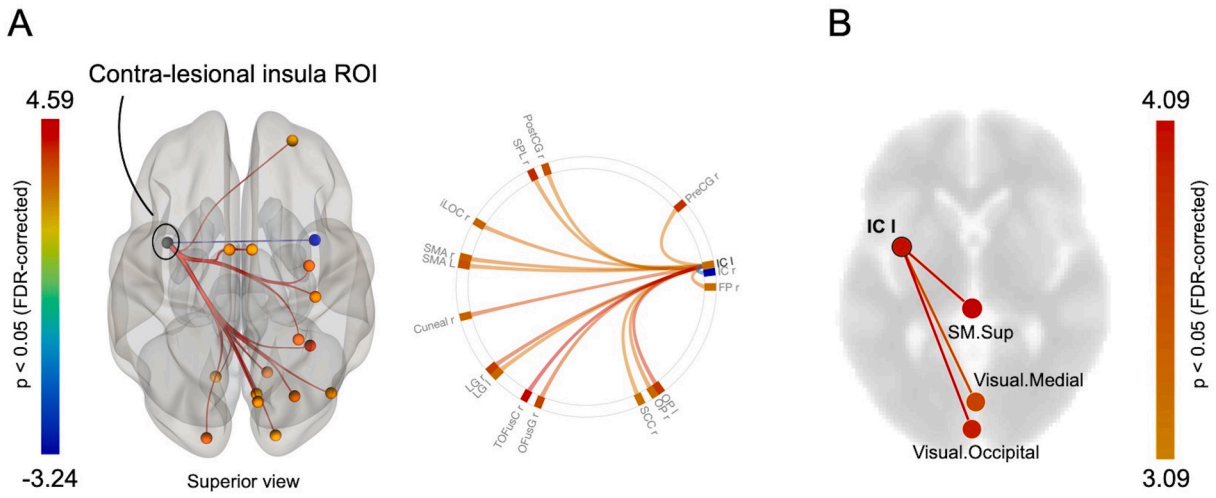


Fig. 3. Tumor-related modulation of insular connectivity in right insular glioma patients versus healthy controls. (A) Contralesional seed-to-ROI map and connectome ring. (B) Contralesional seed-to-network map displayed on an axial slide. Only significant T-values ($p < 0.05$ FDR-corrected) are displayed. IC = insular cortex; SM.Sup = superior sensorimotor.

and Supplementary Table 6). Unlike the insL group, no significant rsFC changes in the ipsilesional insular cortex were found, possibly related to a weaker statistical power (i.e. the number of patients was lower in this group).

All the analyses were performed again by taking into consideration the variables 'sex' and 'handedness' to control for their possible effect on functional connectivity. The results were almost the same as without these factors (see Supplementary Figs. 2 & 3), indicating their minor effect on the functional redistribution described above.

To demonstrate specificity, we examined rsFC changes of 3 mirror control regions. Analyses were performed on both homologous regions (i.e. both hemisphere), in insL and insR groups compared with HCs. Results are displayed in Fig. 4 and Table 2. No significant changes were found for aITG and pTFusC seed-ROIs, either in the contralesional or in the ipsilesional hemisphere ($n = 0$ ROI) for both patient groups. For the insL group, no significant changes were identified for the right, contralesional MidFG seed-ROI, whereas a significant increase of the functional coupling occurred between the left, ipsilesional MidFG and three cortical areas. Similar results were obtained for the insR group. The functional coupling was increased with 2 regions when the left, contralesional MidFG was considered, and with four regions when the right, ipsilesional MidFG was examined. These results indicate that the pattern of functional redistribution identified for the homotopic contralesional insular cortex was not found for other control cortical areas not damaged by the tumors.

4. Discussion

In this hypothesis-driven functional connectivity (FC) study, we found a decrease of the bi-insular FC along with a positive functional modulation of the intact, contralesional one. This pattern of FC changes, specific to the insular cortex, was replicable across both groups of patients. A reasonable interpretation of these physiological variations is that the graded damage of the insula cortex induces a dynamic redeployment of the FC in the homologous one, supporting the concept of homotopic plasticity. This new finding agrees with a recent work in which glioma invasion of insular areas was paralleled by significant and specific changes in the macrostructure of the intact one (Almairac et al., 2018). Collectively, these findings suggest that contralesional structural rewiring supports tumor-induced FC redistribution from the lesioned to the intact insula; in other words, functional and structural plasticity of insular homotopic structures appears to be the two sides of the same coin, at least in the specific context of diffuse-low-grade glioma.

The compensation mechanisms underlying the functional modulations of the homotopic structure are not clearly established. The contralesional functional redistribution we observed for both patient groups concerned sensorimotor and visual networks that are insula-related. In a dynamic view of the brain architecture, the overwhelming of the intact insula could be related to tumor-induced transcallosal disinhibition (Ferbert et al., 1992). According to this concept, in normal physiological circumstances, the homologous areas reciprocally situated in each cerebral hemisphere inhibits each other. When a hemisphere is damaged, the function in the contralateral region is freed from this inhibition. This mechanism could explain the bi-lateralization of the visual and sensorimotor networks which are usually lateralized. To date, however, the transcallosal inhibitory hypothesis has been mainly described for the primary motor system (Boroojerdi et al., 1996; Ferbert et al., 1992; Stefaniak et al., 2020). Furthermore, this theory is challenged by the lack of evidence from studies using dynamic causal modelling (Stefaniak et al., 2020) and by recent findings rather favoring the hypothesis of inter-hemispheric independence (Karolis et al., 2019). Consequently, the increased functional connectivity of the contralesional insula towards bilateral posterior brain areas might be supported by other adaptive mechanisms such as the recruitment of latent or quiescent pathways or an upregulation of underused contralateral networks in normal conditions (Stefaniak et al., 2020).

Interestingly, we demonstrated a contralesional FC redistribution for the visual and sensorimotor networks but not for the salience network, even though an ipsilesional decrease of insular connectivity mainly towards salience areas was evidenced in one group of patients. This pattern of results can be explained by the brain-wide and bilateral organization of the salience network (Seeley et al., 2007; Uddin et al., 2011), for which the anterior insular cortex is thought to be a central node (Uddin, 2015). Speculatively, other networks may help compensating the role of the insula in the salience network, a neuroplasticity strategy recently described as variable neuro-displacement (Jung et al., 2019; Stefaniak et al., 2020). It is therefore possible that the widely distributed feature of the salience network and the potential implication of alternative functional networks weakens the involvement of the intact insula in the functional compensation. In other words, the functional redistribution might be more distributed for the salience network.

Our results showed a decrease of the ipsilesional insular rsFC in one group of patients (insL). Although the depletion of the functional connectivity of the lesioned insula appears intuitive, these findings should be viewed with caution. Indeed, at the cellular level, brain tumors can disturb the integrity of the blood–brain-barrier, disrupt the coupling

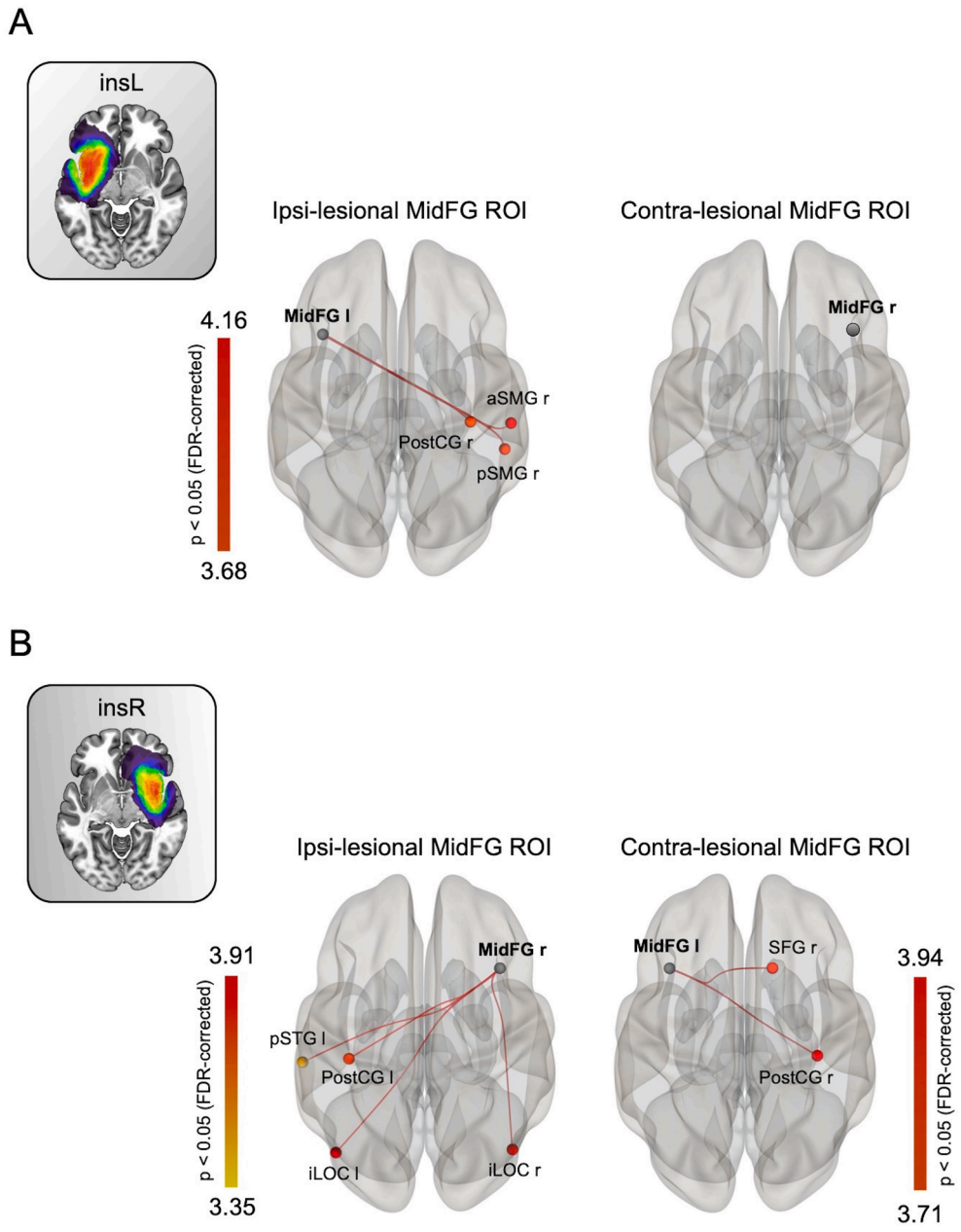


Fig. 4. Modulation of the homologous MidFG connectivity in left and right insular glioma patients versus healthy controls. (A) Ipsi- and contralesional MidFG seed-to-ROI map for left insular glioma patient. (B) Contra- and Ipsilesional seed-to-ROI map for right insular glioma. Only significant T-values ($p < 0.05$ FDR-corrected) are displayed. InsL = left insular glioma patients; InsR = right insular glioma patients; iLOC = inferior lateral occipital; MidFG = middle frontal gyrus; SMG = supramarginal gyrus; postCG = posterior central gyrus; SFG = superior frontal gyrus; STG = superior temporal gyrus.

Table 2
Number of regions with which the functional coupling of the control regions is significantly increased for insL and insR groups compared with HCs.

Control ROIs	Full name	*n* ROIs
insL versus HCs		
aITG l	left inferior temporal gyrus, anterior division	0
aITG r	right inferior temporal gyrus, anterior division	0
pTFusC l	left temporal fusiform cortex, posterior division	0
pTFusC r	right temporal fusiform cortex, posterior division	0
MidFG l	left middle frontal gyrus	3
MidFG r	right middle frontal gyrus	0
insR versus HCs		
aITG l	left inferior temporal gyrus, anterior division	0
aITG r	right inferior temporal gyrus, anterior division	0
pTFusC l	left temporal fusiform cortex, posterior division	0
pTFusC r	right temporal fusiform cortex, posterior division	0
MidFG l	left middle frontal gyrus	2
MidFG r	right middle frontal gyrus	4

Abbreviations: ROI = region of interest.

between neurons and astrocytes, and modify the cerebral flow regulation (Watkins et al., 2014). This phenomenon, referred to as neurovascular uncoupling, may confound the interpretation of resting-state connectivity in brain tumor patients (Agarwal et al., 2016). Besides, brain tumors can also exhibit their own unique and intrinsic BOLD signal profile (Hadjiabadi et al., 2018).

One potential limitation of our study is the generalization of the neuroplasticity strategy we described to other neurological conditions. The slow-growing feature of low-grade gliomas gives the brain the best opportunities to reorganize its networks over time, in parallel to tumor infiltration (Desmurget et al., 2007; Yuan et al., 2019). Whether homotopic plasticity may occur in sudden neurological diseases such as stroke injury or other neurological events remains to date unclear. While a very few studies have succeeded to identify such mirroring changes, the conclusions were typically based on a low number of patients not allowing to generalize this pattern as a common adaptive mechanism. In addition, the triggering factors favoring this strategy of functional remodeling over others (such as perilesional or intra-hemispheric

changes) is not established. For example, among different possible accounts, homotopic plasticity might be preferred when the amount of damage of a given cortical area is too wide to be compensated for by the surrounding, intact cortex – as in our study in which the insula was massively invaded. Consequently, additional works are needed to further our understanding about the mechanistic aspects of homotopic functional plasticity, ideally across multiple pathophysiological contexts.

Another limitation relates to the undemonstrated link between homotopic plasticity and functional compensation of insular functions. Although patients almost systematically benefit from a neuropsychological assessment in our center before any surgical treatment, the behavioral tasks classically used do not allow to tap the functions specific to the insular cortex which are multiple and complex. As a result, a valuable extension of the present study would be to quantify the behavior value of the identified dynamic changes using a large panel of tasks gauging the supposed emotion, cognitive and sensorimotor functions of the insular structures.

Finally, a last note of caution must be added regarding the matching between the control group and the patient group. First, while all MRI acquisitions were performed with a 3 T scanner for the control group, some of them were performed with a 1.5 T machine for the patient group. Although 'scanner difference' was taken into consideration in the analyses, we cannot rule out the possibility that the results might have been affected by the use of two magnets, especially weakening those from the right insular group in which 6 out of 16 patients were scanned with a 1.5 T scanner. However, our research group has recently shown that using different magnets (with the same scanners and the same acquisition parameters as in this study) has no significant impact on the functional connectivity results (Coget et al., 2018). Second, some patients in the patient group were left-handed while all control participants were right-handed. However, no statistical differences were observed between the patient group and the control group, and the lack of perfect matching did not modulate the final results. Third, all patients and none of the heahly controls were under levetiracetam at the time of the fMRI measurements. This factor may limit comparability between groups and might represent a systematic bias.

5. Conclusion

In summary, this study has capitalized on a relatively large sample of patients with insula-centered gliomas. The findings indicate that widespread unilateral infiltration of the insular structures decreases the functional interactions of the lesioned insula while increasing those of the contralesional one, especially with areas of the visual and sensorimotor networks. This suggests that homotopic plasticity is a central adaptive mechanism that participates to the high degree of functional compensation usually observed in low-grade glioma patients, even after neurosurgery. This pattern of functional redistribution, as well as its triggering factors, needs to be further characterized in future studies.

Disclosures

The authors report no disclosures relevant to the manuscript. No targeted funding reported.

CRediT authorship contribution statement

Fabien Almairac: Conceptualization, Methodology, Formal analysis, Visualization, Writing - original draft. **Jeremy Deverdun:** Conceptualization, Methodology, Formal analysis. **Jérôme Cochereau:** Conceptualization, Methodology, Formal analysis. **Arthur Coget:** Conceptualization, Methodology, Formal analysis. **Anne-Laure Lemaitre:** Investigation, Resources. **Sylvie Moritz-Gasser:** Investigation, Resources. **Hugues Duffau:** Writing - review & editing. Guillaume Herbet: Supervision, Conceptualization, Writing - review & editing.

Declaration of Competing Interest

The authors declare that they have no known competing financial interests or personal relationships that could have appeared to influence the work reported in this paper.

Appendix A. Supplementary data

Supplementary data to this article can be found online at https://doi.org/10.1016/j.nicl.2021.102571.

References

Agarwal, S., Sair, H.I., Yahyavi-Firouz-Abadi, N., Airan, R., Pillai, J.J., 2016. Neurovascular uncoupling in resting state fMRI demonstrated in patients with primary brain gliomas. J. Magn. Reson. Imaging 43 (3), 620–626. https://doi.org/10.1002/jmri.25012.

Almairac, F., Duffau, H., Herbet, G., 2018. Contralesional macrostructural plasticity of the insular cortex in patients with glioma: A VBM study. Neurology 91 (20), e1902–e1908. https://doi.org/10.1212/WNL.0000000000006517.

Almairac, F., Herbet, G., Moritz-Gasser, S., de Champfleur, N.M., Duffau, H., 2015. The left inferior fronto-occipital fasciculus subserves language semantics: a multilevel lesion study. Brain Struct. Funct. 220 (4), 1983–1995. https://doi.org/10.1007/s00429-014-0773-1.

Behzadi, Y., Restom, K., Liau, J., Liu, T.T., 2007. A component based noise correction method (CompCor) for BOLD and perfusion based fMRI. Neuroimage 37 (1), 90–101. https://doi.org/10.1016/j.neuroimage.2007.04.042.

Boroojerdi, B., Diefenbach, K., Ferbert, A., 1996. Transcallosal inhibition in cortical and subcortical cerebral vascular lesions. J. Neurol. Sci. 144 (1-2), 160–170. https://doi.org/10.1016/S0022-510X(96)00222-5.

Cauda, F., D'Agata, F., Sacco, K., Duca, S., Geminiani, G., Vercelli, A., 2011. Functional connectivity of the insula in the resting brain. Neuroimage 55 (1), 8–23. https://doi.org/10.1016/j.neuroimage.2010.11.049.

Cerliani, L., Thomas, R.M., Jbabdi, S., Siero, J.C.W., Nanetti, L., Crippa, A., Gazzola, V., D'Arceuil, H., Keysers, C., 2012. Probabilistic tractography recovers a rostrocaudal trajectory of connectivity variability in the human insular cortex. Hum. Brain Mapp. 33 (9), 2005–2034. https://doi.org/10.1002/hbm.v33.910.1002/hbm.21338.

Cochereau, J., Deverdun, J., Herbet, G., Charroud, C., Boyer, A., Moritz-Gasser, S., Le Bars, E., Molino, F., Bonafé, A., Menjot de Champfleur, N., Duffau, H., 2016. Comparison between resting state fMRI networks and responsive cortical stimulations in glioma patients. Hum. Brain Mapp. 37 (11), 3721–3732. https://doi.org/10.1002/hbm.v37.1110.1002/hbm.23270.

Coget, A., Deverdun, J., Bonafé, A., van Dokkum, L., Duffau, H., Molino, F., Le Bars, E., de Champfleur, N.M., 2018. Transient immediate postoperative homotopic functional disconnectivity in low-grade glioma patients. Neuroimage Clin 18, 656–662. https://doi.org/10.1016/j.nicl.2018.02.023.

(Bud) Craig, A.D., 2009. How do you feel–now? The anterior insula and human awareness. Nat. Rev. Neurosci. 10 (1), 59–70. https://doi.org/10.1038/nrn2555.

Desikan, R.S., Ségonne, F., Fischl, B., Quinn, B.T., Dickerson, B.C., Blacker, D., Buckner, R.L., Dale, A.M., Maguire, R.P., Hyman, B.T., Albert, M.S., Killiany, R.J., 2006. An automated labeling system for subdividing the human cerebral cortex on MRI scans into gyral based regions of interest. Neuroimage 31 (3), 968–980. https://doi.org/10.1016/j.neuroimage.2006.01.021.

Desmurget, M., Bonnetblanc, F., Duffau, H., 2007. Contrasting acute and slow-growing lesions: a new door to brain plasticity. Brain 130, 898–914. https://doi.org/10.1093/brain/awl300.

Dionisio, S., Mayoglou, L., Cho, S.-M., Prime, D., Flanigan, P.M., Lega, B., Mosher, J., Leahy, R., Gonzalez-Martinez, J., Nair, D., 2019. Connectivity of the human insula: A cortico-cortical evoked potential (CCEP) study. Cortex 120, 419–442. https://doi.org/10.1016/j.cortex.2019.05.019.

Duffau, H., 2005. Lessons from brain mapping in surgery for low-grade glioma: insights into associations between tumour and brain plasticity. Lancet Neurol. 4 (8), 476–486. https://doi.org/10.1016/S1474-4422(05)70140-X.

Duffau, H., Taillandier, L., Gatignol, P., Capelle, L., 2006. The insular lobe and brain plasticity: Lessons from tumor surgery. Clin. Neurol. Neurosurg. 108 (6), 543–548. https://doi.org/10.1016/j.clineuro.2005.09.004.

Ferbert, A., Priori, A., Rothwell, J.C., Day, B.L., Colebatch, J.G., Marsden, C.D., 1992. Interhemispheric inhibition of the human motor cortex. J. Physiol. (Lond.) 453, 525–546. https://doi.org/10.1113/jphysiol.1992.sp019243.

Friston, K.J., Holmes, A.P., Poline, J.-B., Grasby, P.J., Williams, S.C.R., Frackowiak, R.S. J., Turner, R., 1995. Analysis of fMRI time-series revisited. Neuroimage 2 (1), 45–53. https://doi.org/10.1006/nimg.1995.1007.

Gauthier, L.V., Taub, E., Perkins, C., Ortmann, M., Mark, V.W., Uswatte, G., 2008. Remodeling the brain plastic structural brain changes produced by different motor therapies after stroke. Stroke 39 (5), 1520–1525. https://doi.org/10.1161/STROKEAHA.107.502229.

Glickman, M.E., Rao, S.R., Schultz, M.R., 2014. False discovery rate control is a recommended alternative to Bonferroni-type adjustments in health studies. J. Clin. Epidemiol. 67 (8), 850–857. https://doi.org/10.1016/j.jclinepi.2014.03.012.

Hadjiabadi, D.H., Pung, L., Zhang, J., Ward, B.D., Lim, W.-T., Kalavar, M., Thakor, N.V., Biswal, B.B., Pathak, A.P., 2018. Brain tumors disrupt the resting-state connectome. Neuroimage Clin. 18, 279–289. https://doi.org/10.1016/j.nicl.2018.01.026.

Hallquist, M.N., Hwang, K., Luna, B., 2013. The nuisance of nuisance regression: spectral misspecification in a common approach to resting-state fMRI preprocessing reintroduces noise and obscures functional connectivity. Neuroimage 82, 208–225. https://doi.org/10.1016/j.neuroimage.2013.05.116.

Herbet, G., Maheu, M., Costi, E., Lafargue, G., Duffau, H., 2016. Mapping neuroplastic potential in brain-damaged patients. Brain 139 (3), 829–844. https://doi.org/10.1093/brain/awv394.

Jung, J., Rice, G.E., Lambon Ralph, M.A., 2019. The neural bases of resilient cognitive systems: Evidence of variable neuro-displacement in the semantic system. bioRxiv 716266. doi: 10.1101/716266.

Karolis, V.R., Corbetta, M., Thiebaut de Schotten, M., 2019. The architecture of functional lateralisation and its relationship to callosal connectivity in the human brain. Nat. Commun. 10 (1) https://doi.org/10.1038/s41467-019-09344-1.

Louis, D.N., Perry, A., Reifenberger, G., von Deimling, A., Figarella-Branger, D., Cavenee, W.K., Ohgaki, H., Wiestler, O.D., Kleihues, P., Ellison, D.W., 2016. The 2016 World Health Organization Classification of Tumors of the Central Nervous System: a summary. Acta Neuropathol. 131 (6), 803–820. https://doi.org/10.1007/s00401-016-1545-1.

Nieuwenhuys, R., 2012. The insular cortex: a review. Prog. Brain Res. 195, 123–163. https://doi.org/10.1016/B978-0-444-53860-4.00007-6.

Pang, X.-M., Liang, X.-L., Zhou, X., Liu, J.-P., Zhang, Z., Zheng, J.-O., 2020. Alterations in intra- and internetwork functional connectivity associated with levetiracetam treatment in temporal lobe epilepsy. Neurol. Sci. 41 (8), 2165–2174. https://doi.org/10.1007/s10072-020-04322-8.

Power, J.D., Mitra, A., Laumann, T.O., Snyder, A.Z., Schlaggar, B.L., Petersen, S.E., 2014. Methods to detect, characterize, and remove motion artifact in resting state fMRI. Neuroimage 84, 320–341. https://doi.org/10.1016/j.neuroimage.2013.08.048.

Rice, G.E., Caswell, H., Moore, P., Lambon Ralph, M.A., Hoffman, P., 2018. Revealing the dynamic modulations that underpin a resilient neural network for semantic cognition: an fMRI investigation in patients with anterior temporal lobe resection. Cereb. Cortex 28, 3004–3016. https://doi.org/10.1093/cercor/bhy116.

Rorden, C., Karnath, H.-O., Bonilha, L., 2007. Improving lesion-symptom mapping. J. Cogn. Neurosci. 19 (7), 1081–1088. https://doi.org/10.1162/jocn.2007.19.7.1081.

Seeley, W.W., Menon, V., Schatzberg, A.F., Keller, J., Glover, G.H., Kenna, H., Reiss, A.L., Greicius, M.D., 2007. Dissociable intrinsic connectivity networks for salience processing and executive control. J. Neurosci. 27 (9), 2349–2356. https://doi.org/10.1523/JNEUROSCI.5587-06.2007.

Stefaniak, J.D., Halai, A.D., Lambon Ralph, M.A., 2020. The neural and neurocomputational bases of recovery from post-stroke aphasia. Nat. Rev. Neurol. 16 (1), 43–55. https://doi.org/10.1038/s41582-019-0282-1.

Uddin, L.Q., 2015. Salience processing and insular cortical function and dysfunction. Nat. Rev. Neurosci. 16 (1), 55–61. https://doi.org/10.1038/nrn3857.

Uddin, L.Q., Supekar, K.S., Ryali, S., Menon, V., 2011. Dynamic reconfiguration of structural and functional connectivity across core neurocognitive brain networks with development. J. Neurosci. 31 (50), 18578–18589. https://doi.org/10.1523/JNEUROSCI.4465-11.2011.

Voytek, B., Davis, M., Yago, E., Barceló, F., Vogel, E.K., Knight, R.T., 2010. Dynamic Neuroplasticity after Human Prefrontal Cortex Damage. Neuron 68 (3), 401–408. https://doi.org/10.1016/j.neuron.2010.09.018.

Watkins, S., Robel, S., Kimbrough, I.F., Robert, S.M., Ellis-Davies, G., Sontheimer, H., 2014. Disruption of astrocyte-vascular coupling and the blood-brain barrier by invading glioma cells. Nat. Commun. 5, 4196. https://doi.org/10.1038/ncomms5196.

Whitfield-Gabrieli, S., Nieto-Castanon, A., 2012. Conn: a functional connectivity toolbox for correlated and anticorrelated brain networks. Brain Connect. 2 (3), 125–141. https://doi.org/10.1089/brain.2012.0073.

Yordanova, Y.N., Cochereau, J., Duffau, H., Herbet, G., 2019. Combining resting state functional MRI with intraoperative cortical stimulation to map the mentalizing network. Neuroimage 186, 628–636. https://doi.org/10.1016/j.neuroimage.2018.11.046.

Yuan, B., Zhang, N., Yan, J., Cheng, J., Lu, J., Wu, J., 2019. Resting-state functional connectivity predicts individual language impairment of patients with left hemispheric gliomas involving language network. Neuroimage Clin. 24, 102023. https://doi.org/10.1016/j.nicl.2019.102023.